Locating and quantifying damage in beam-like structures using modal flexibility-based deflection changes

N.T. Le[a, c], A. Nguyen[a,b,*], D.P. Thambiratnam[a], T.H.T Chan[a], T. Khuc[c]

[a] Queensland University of Technology, Australia; [b] University of Southern Queensland, Australia; [c] National University of Civil Engineering, Vietnam; [*] Email: andy.nguyen@usq.edu.au; a66.nguyen@qut.edu.au

Abstract

This paper presents an enhanced method to locate and quantify damage in beam-like structures using changes in deflections estimated from modal flexibility (MF) matrices. The method is developed from explicit relationship between a series of MF-based deflection change vectors and the damage characteristics. Based on this, three damage locating criteria are defined and used to detect and locate damage. Once the damage is located, its severity is estimated conveniently from a closed-form function. The capability of the proposed method is examined through numerical and experimental verifications on a steel beam model. The result shows that the method accurately locates and quantifies damage under various scenarios using a few modes of vibration, with satisfactory or even better results compared to those obtained from traditional static deflection-based method. The performance of the proposed method is also compared with three well-known vibration-based damage detection methods using changes in modal flexibility and modal strain energy. It is found that the proposed method outperformed the other three methods, especially for multiple damage cases. As beams can represent various structural components, the proposed method provides a promising damage identification tool targeting the application to real-life structures.

Keywords: Damage detection; In-service monitoring; Modal flexibility change; Modal flexibility-based deflection; Damage quantification; Beam-like structures

1. Introduction

Structural damage identification has been recognized as an essential aspect in the health monitoring of important civil-engineering structures to reveal the onset of damage and enable appropriate retrofitting measures to be taken before the damage escalates to an extent that can make the structures unserviceable [1,

2]. Over the past few decades, research on damage detection (DD) has received considerable attention as evidenced from a large number of methods developed and studied utilizing various global structural responses, which can be classified into dynamic (such as frequencies, mode shapes and their derivatives) and static (such as static deflections and strains) categories.

Among the DD methods using dynamic responses, modal flexibility (MF) has become one of the most promising damage descriptors owing to its sensitivity to damage [3-9]. The merit can be explained by the fact that MF combines natural frequencies and mode shapes, making it more sensitive to damage detection than the methods using either of the two modal parameters separately [8]. In addition, since the MF computation converges rapidly with increasing natural frequencies, a reasonable representation of the flexibility can be obtained from a few lower modes of vibration [3, 9, 10]. This provides a practical advantage for the DD solutions as obtaining high-order modal data has been challenging in real civil structures. Another advantage is that since the low-order modal parameters can now be conveniently extracted from vibration measurements under operational conditions [11], the MF-based DD approach is ideally suited for continuous monitoring. The method has been explored for damage detection in a wide range of structures including bridges [5, 9, 12-16], shear buildings [6, 17, 18], and concrete gravity dams [19], to name a few. However, since there is no explicit mathematical formulation between the MF changes and the damage extent [3], it has not been straightforward to quantify the damage from MF [17, 18, 20].

In the DD approach utilizing static responses, static deflection change has been one of the most popular damage features [21-25]. Since static deflection is directly related to the structural stiffness as evidenced from the principles of structural mechanics, it is usually suitable for damage quantification providing that stiffness reduction is the main source of structural damage in civil structures. Recently, the present authors developed a new deflection-based damage detection (DBDD) method based on explicit relationships between the static deflection changes and the damage characteristics for Euler-Bernoulli beams [25]. This method is among a few DBDD methods that can locate and quantify damage directly from the measured deflection change without relying on an optimization algorithm. However, this method and many other DBDD methods require the deflections to be measured under specific applied loads so that their relationship with the structural stiffness can be exploited. This inadvertently limits DBDD methods to controlled load test applications only, meaning

the methods are not suitable for continuous monitoring of in-service structures. One way to circumvent this limitation is to use the pseudo deflections that are not measured but estimated indirectly from modal flexibility [6, 7, 17, 18, 26, 27]. The basic idea behind this approach is that the column flexibility at a measured degree of freedom (DOF) is physically the static displacement vector obtained from an applied unit load at that DOF. Therefore, from a measured MF matrix one can estimate the MF-based deflections under arbitrary virtual point loads acting at the DOFs without the need of applying an actual load on the structure. However, current methods using MF-based deflections can only detect and locate damage in beam-like structures [7, 26], while those capable of quantifying damage are only applicable for shear buildings [6, 17, 18]. There is therefore a real need to explore the ability of MF-based deflections to quantify damage in beam-like structures, as seen in many real structures such as girder bridges and building frame systems.

This paper presents an enhanced deflection-based damage detection method that can enable the use of MF-based deflections to locate and quantify damage in beam-like structures and thereby extend the application of deflection-based methods toward in-service monitoring. In addition, by using MF-based deflection instead of the direct MF data, damage quantification becomes possible. The rest of this paper is organized as follows. First presented is the theory on the developed method and its enhanced components for locating and quantifying damage under different scenarios. Next, comprehensive numerical, experimental and comparative studies on a steel beam structure are carried out to examine the capacities of the method. The paper concludes with summary and final remarks on the study.

2. Theory

2.1. Estimation of deflections from modal flexibility matrices

The flexibility matrix F, which is the inverse of the system stiffness matrix, can be constructed from the measured modal parameters as follows [3, 10]:

$$\mathbf{F} = \sum_{i=1}^{N} \frac{1}{\omega_i^2} \phi_i \phi_i^{\mathrm{T}} \tag{1}$$

where, ϕ_i and ω_i are the ith mass-normalised mode shape and modal frequency, respectively; N is the number of DOFs of the structure. Equation (1) reveals that flexibility is inversely proportional to the square of modal frequencies, implying that it can be estimated with sufficient accuracy by using a few early modes of vibration.

3

1   The modal flexibility matrix **MF** using n lower modes can be presented by:

$$\mathbf{MF} = \sum_{i=1}^{n} \frac{1}{\omega_i^2} \phi_i \phi_i^{\mathrm{T}} \tag{2}$$

2   After obtaining the MF matrix from Eq. (2), the static deflection of the structure under an arbitrary virtual

3   static point load (**f**) acting at the measurement DOFs can be estimated as follows [28]:

$$u = \mathbf{F}\,\mathbf{f} \approx \mathbf{MF}\,\mathbf{f} \tag{3}$$

4   The damage-induced deflection change can then be estimated from the modal flexibility change (**MFC**) as:

$$DC = u^{\mathrm{d}} - u^{\mathrm{h}} \approx \left(\mathbf{MF}^{\mathrm{d}} - \mathbf{MF}^{\mathrm{h}}\right)\mathbf{f} = \mathbf{MFC}\,\mathbf{f} \tag{4}$$

5   where, the superscriptions "d" and "h" denote the damaged and undamaged (healthy) states of the structure,

6   respectively. The damage-induced relative deflection change (RDC) can then be estimated from the relative

7   flexibility change (**RFC**) matrix by the following operations:

$$RDC = DC./u^{\mathrm{h}} \approx \left(\mathbf{MFC}./\mathbf{MF}^{\mathrm{h}}\right)\mathbf{f} = \mathbf{RFC}\,\mathbf{f} \tag{5}$$

8   where the notation "./" denotes the elemental-wise division. If **f** is a unit point load (UPL) acting at the ith DOF,

9   the MF-based DC parameter estimated from Eq. (4) is simply the ith column of the MFC matrix (Fig. 1a).

10   Similarly, the MF-based RDC obtained from Eq. (5) is the ith column of the **RFC** matrix. Therefore, a series

11   of MF-based DC and RDC vectors under multiple UPLs can be extracted from the **MFC** and **RFC** matrices

12   without the need to conduct multiple static deflection tests.

13   **2.2. The enhanced deflection-based damage detection method**

14   This section presents main elements of the enhanced DBDD method that is applicable for a series of MF-based

15   deflections under multiple UPLs. In the original DBDD method developed by the present authors for Euler-

16   Bernoulli beams [25], theoretical mathematical formulas of the static DC with respect to the damage

17   characteristics was developed for a specific UPL at mid-span of simply supported (SS) beams (or at the free-

18   end of cantilever beams). In this section, the formulas will be redeveloped for an arbitrary UPL following an

19   analogous procedure but truncated for brevity. As in the original method, the enhanced method developed

20   herein considers linear damage situations in which the initially linear-elastic structure remains linear-elastic

21   after damage [29].

2.2.1. Damage locating concept from MF-based deflection changes

Consider a simply supported beam with constant flexural stiffness EI in the undamaged state. Under a UPL acting at location x_L, the undamaged deflection of the beam can be formulated by Macaulay method [30], or by Virtual Work [28] as follows:

$$u^h(x, x_L) = \frac{1}{12EI} u_0(x, x_L) \tag{6}$$

$$u_0(x, x_L) = 2\langle x - x_L \rangle^3 + 2(1 - \frac{x_L}{L})[x_L(2L - x_L)x - x^3] \tag{7}$$

where, $u_0(x, x_L)$ is a geometrical deflection function; L is the beam length; the angle bracket $\langle \rangle$ should be replaced by ordinary parentheses ( ) when $x \geq x_L$, and by zero when $x < x_L$. It is assumed that the beam is later subjected to a single damage at segment $a \leq x \leq a + b$ (Fig. 1b). Under the same UPL acting at $x = x_L$ before and after damage, the damage-induced DC can be formulated from the principle of Virtual Work by:

$$DC(x, x_L) = \beta \frac{1}{12EI} g(x)\, h(x_L) \tag{8}$$

$$g(x) = B_1 x\, H(a - x) + B_2(L - x)H(x - a - b) \tag{9}$$

$$h(x_L) = \frac{2}{L}[x_L\, H(a - x_L) + (L - x_L)H(x_L - a - b)] \tag{10}$$

where, $\beta = \alpha/(1 - \alpha)$ is a damage severity derivative, $0 \leq \alpha < 1$ is the damage severity coefficient; $g(x)$ and $h(x_L)$ are two pulse functions with respect to the beam inspection coordinates x and the UPL position x_L, respectively; $H(.)$ is the Heaviside step function, whose value is zero for negative argument and one for zero or positive arguments; B_1 and B_2 are scalar functions containing only the damage location information as presented in Eq. (11) bellow:

$$x_L \leq a: \ B_1 = -\frac{2}{L}[(L - a - b)^3 - (L - a)^3];$$
$$B_2 = \frac{b}{L}[(2a + b)(3L - 2a - 2b) - 2a^2] \tag{11a}$$

$$x_L \geq a + b: \ B_1 = \frac{b}{L}[(2a + b)(3L - 2a - 2b) - 2a^2];$$
$$B_2 = \frac{2}{L}[(a + b)^3 - a^3] \tag{11b}$$

Recalling Eq. (4), it can be ascertained that each column of the MFC matrix represents a MF-based $DC(x, x_L)$ vector that follows the mathematical function presented in Eq. (8). There are three important observations that can be made from Eqs. (8) - (10). First, for a specific UPL ($x_L = $ constant), the $DC(x)$ plot comprises two linear

1 portions starting from the supports towards the damage segment. Second, for a specific UPL position, the

2 $DC(x)$ reaches its peak when x approaches the damaged region $(a, a + b)$. The third observation is that for each

3 measurement DOF (x = constant), the $DC(x_L)$ intensities are highest when the UPL is applied at $x_L = a$ or $a +$

4 b, and get smaller when the load is applied far apart. In other words, $DC(x, x_L = a)$ and $DC(x, x_L = a+b)$ are the

5 most outlier plots among the measured DCs (Fig. 1c).

6
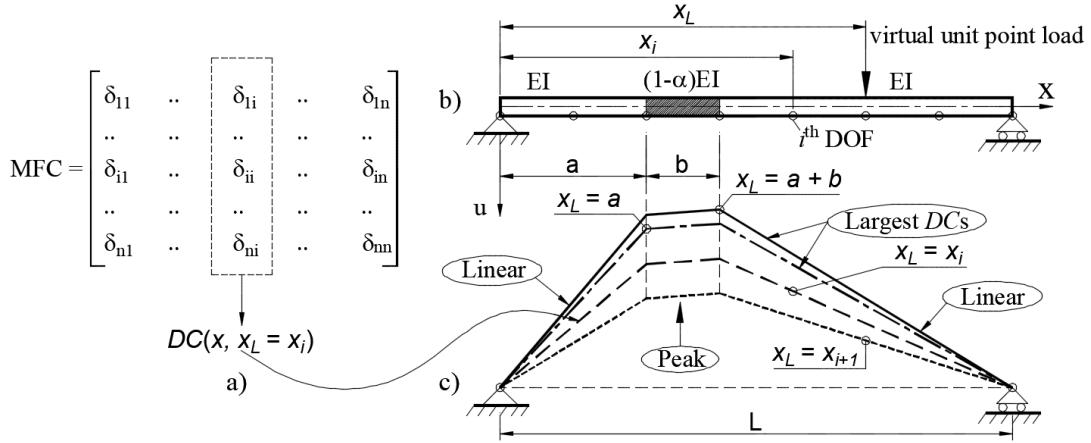
7
8 Fig. 1. The enhanced damage-locating concept: (a) Schematic of the MF-based DC, (b) The beam configuration, (c) DC
9 plots under different point loads and the three damage-locating criteria (in ovals)

10 It should be emphasised that the first two observations were used in [25] as the two damage locating criteria.

11 However, as reported by the present authors in the paper, due to unavoidable measurement noise, the linearity

12 of the DC plots might become less obvious in early damage scenarios causing certain difficulties in identifying

13 the damage. In this situation, the third observation provides a useful additional damage locating tool. It is

14 therefore named here as the third criterion in the enhanced damage-locating concept, in addition to the two

15 criteria developed in the original DBDD method.

16 **2.2.2. Damage quantification using MF-based relative deflection changes**

17 Recalling Eq. (5), the MF-based RDC parameter can be presented in a mathematical form on the substitution

18 of Eq. (6) and (8) as follows:

$$RDC(x, x_L) = DC(x, x_L)./u^h(x, x_L) = \beta\ RDC^{50\%}(x, x_L) \tag{12}$$

19 where, "./" denotes the elemental-wise vector division, $RDC^{50\%}$ is a scalar function calculated from Eqs. (7),

20 (9), and (10) by:

$$RDC^{50\%}(x, x_L) = [g(x)\ h(x_L)]./u_0(x, x_L) \tag{13}$$

6

1   It can be observed from (12) that the measured RDC differs from $RDC^{50\%}$ by a scalar multiplier, and that

2   $RDC^{50\%}$ is physically a measured RDC when the scalar β is equal to 1, or $\alpha = 50\%$. $RDC^{50\%}$ is therefore

3   considered as a referenced relative deflection change, which is calculated from Eq. (13) after the damage is

4   located. It should be noted that the referenced $RDC^{50\%}$ does not necessarily represent a real damage state, but

5   rather an intermediate parameter connecting the measured RDC to the unknown damage severity coefficient.

6   As evidenced from Eq. (12), the measured RDC is separated into two independent parameters with respect to

7   the damage characteristics: (i) the damage severity coefficient contained in the scalar β, and (ii) the damage

8   location information stored in the $RDC^{50\%}$ function. Therefore, once $RDC^{50\%}$ is determined, the damage

9   severity information can be conveniently extracted from the measured RDC as follows:

$$\beta(x_L) = \overline{DSC}(x, x_L), \qquad x \notin (a, a + b) \tag{14}$$

10 where, $DSC(x, x_L)$ is the damage severity consistency (DSC) function [25] calculated at the inspection locations

11 for each of the UPLs:

$$DSC(x, x_L) = RDC(x, x_L)./RDC^{50\%}(x, x_L), \qquad x \notin (a, a + b) \tag{15}$$

12 Subsequently, the damage severity coefficient is calculated for a specific UPL by:

$$\alpha(x_L) = \frac{\beta(x_L)}{1 + \beta(x_L)} \tag{16}$$

13 The damage quantification procedure from Eq. (13) to Eq. (16) can be repeated for each of the MF-based RDC

14 vectors. After eliminating abnormal $\alpha(x_L)$ values at DOFs which are probably subjected to high measurement

15 noise, the final damage severity is derived by averaging the $\alpha(x_L)$ values at DOFs that provide consistent

16 results.

17 **2.2.3. Locating and quantifying double damage**

18 Fig. 2a illustrates the damage locating concept of the original DBDD method for a double damage scenario

19 [25]. It shows that the damage can be identified at the abrupt changes of the DC plot under the UPL acting at

20 mid-span ($x_L=L/2$), and that the DC is a superposition of the two single deflection change components, viz.

21 DC_1 and DC_2, which are induced by each of the damages separately. As reported in [25], the method has some

22 difficulties in detecting the less severe damage, e.g. at $(a_1, a_1 + b_1)$, which is located far from the static UPL.

23 This can be explained herein by the third damage-locating criterion (section 2.2.1) that under this UPL, the

7

1. DC_1 intensity is too small compared to DC_2. As a result, the peak at the less severe damage on the collective

2. DC plot becomes less definite and can be easily masked by measurement noise.

3. In the present enhanced DBDD method, this shortcoming can be overcome by inspecting all available MF-

4. based DC vectors. As illustrated in Fig. 2b, the intensity of the MF-based DC plots at the damage vicinity

5. becomes higher when the UPL is closer to that damage and hence presents more definite abrupt changes to

6. facilitate the identification of hidden damage. The enhanced method is therefore robust compared to the

7. original counterpart in dealing with double damage cases.

8. After the damage location identifiers (a_i, b_i) are determined, the scalars B_{1i}, B_{2i} are calculated from Eqs. (11),

9. and the damage severity consistency functions $DSC_i(x)$ are calculated using Eq. (17) for each of the damage

10. locations as follows:

$$DSC_i(x, x_L) = \frac{RDC(x, x_L)}{RDC_i^{50\%}(x, x_L)} \,, \qquad x \notin (a_i, a_i + b_i), \qquad i = 1,2 \tag{17}$$

11. where, the baseline $RDC_i^{50\%}$ functions are pre-calculated from Eq. (13) for each of the damage locations.

12. a)   b)
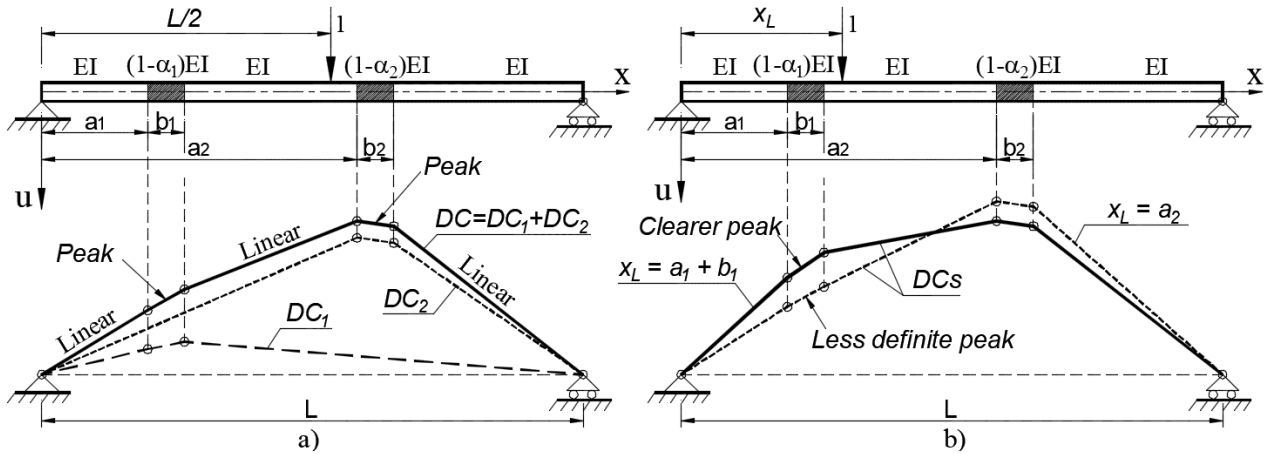
13. Fig. 2. (a) Original damage-locating concept, (b) Enhanced damage-locating concept

14. The damage severity derivatives β_i are then estimated by solving the pair linear equations:

$$\begin{cases} (1/DSC_{11})\, \beta_1(x_L) + (1/DSC_{12})\, \beta_2(x_L) = 1 \,, & x \leq a_1 \\ (1/DSC_{21})\, \beta_1(x_L) + (1/DSC_{22})\, \beta_2(x_L) = 1 \,, & x \geq a_2 + b_2 \end{cases} \tag{18}$$

15. where,

$$\begin{cases} DSC_{1i} = \overline{DSC_{1i}(x, x_L)} = \overline{RDC(x, x_L)/RDC_i^{50\%}(x, x_L)} \,, & 0 < x \leq a_1, i = 1,2 \\ DSC_{2i} = \overline{DSC_{2i}(x, x_L)} = \overline{RDC(x, x_L)/RDC_i^{50\%}(x, x_L)} \,, & a_2 + b_2 \leq x < L, i = 1,2 \end{cases} \tag{19}$$

8

1 The damage severity coefficients are then calculated from Eq. (16) for each of the two damaged elements.

2 Finally, by visiting all available MF-based *RDC*s, the damage severities are drawn by the averaging technique.

3 **3. Numerical simulation through finite element model of a 2.5m steel beam**

4 In order to demonstrate the feasibility of the proposed method, numerical simulation was carried out on a finite

5 element model (FEM) of a 2.5m SS beam (Fig. 3). The cross-section of the beam is a simplified AS/NZS grade

6 C450 cold formed Duragal 75×40×4 CC. This FEM was validated based on static and modal tests in the

7 previous studies of present authors [25]. Details of the modal tests will be presented later in section 4. Five

8 damage scenarios were simulated by cutting the two flanges by 1.5mm width and varying depths (Table 1).

9 These sectional cuts will cause stiffness reduction on the surrounding area, which can be assessed for an

10 equivalent damaged beam segment spreading three times the beam high [31]. The elemental damage severity

11 coefficients for each damage scenarios estimated numerically and experimentally using the original DBDD

12 method in [25] will serve as baseline to evaluate the performance of the proposed method in this paper (Table

13 3 and Table 5).

14
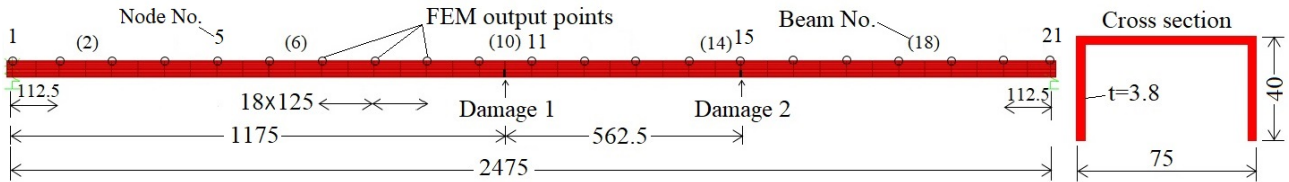
15 Fig. 3. The beam finite element model (E=216 GPa, ν=0.3, ρ=7850 kg/m³, dimensions are in mm)

16 Table 1. Damage scenario definition

Damage case	Vertical depth of the cuts	
	Damage 1	Damage 2
D1.1	8.5 mm	
D1.2	12.5 mm	N/A
D1.3	18.0 mm	
D1.4	Same as D1.3	12.0 mm
D1.5	Same as D1.3	18.0 mm

17 Intact mode shapes and changes in natural frequencies due to the damage are shown in Fig. 4 and Table 2. The

18 frequencies were found to decrease gradually, suggesting the presence of progressive damage. The first three

19 modes were used to construct the MF matrices and estimate the MF-based deflections. DD results for a typical

1 single damage (D1.1) and a double damage (D1.4) cases are presented in Fig. 5. Results for other damage

2 scenarios were found to be similar and hence are not presented for brevity. In addition, for simplicity, the RDC

3 and $RDC^{50\%}$ plots are omitted and only the ratio between them (the consistency functions DSC) are plotted.

4 Regarding the single damage case (Fig. 5a), the MF-based DCs under various UPLs (1kN in magnitude) acting

5 at different nodes clearly reveal a peak between the linear portions. The figure also depicts that the intensity

6 of the DC plots gradually increases when the UPL is closer to node No.10 and 11. Therefore, the most outlier

7 DCs were found to be under the UPLs acting at nodes 10 and 11. From the proposed damage-locating criteria,

8 the damage was correctly located at the beam element No.10. The 2nd and 3rd rows of Fig. 5a then illustrate

9 nearly constant DSC plots and very close estimations of the damage extents under three selected UPLs.

10 For the double damage case D1.4, the first damage can be identified from all MF-based DC plots, while only

11 those produced by the UPLs acting at nodes 15 and 17 can reveal the second damage with definite results (Fig.

12 5b). This demonstrates the advantage of the enhanced DD method over the original one [25] since in the

13 original approach, using only one DC can miss one of the damages. The average of the estimations under all
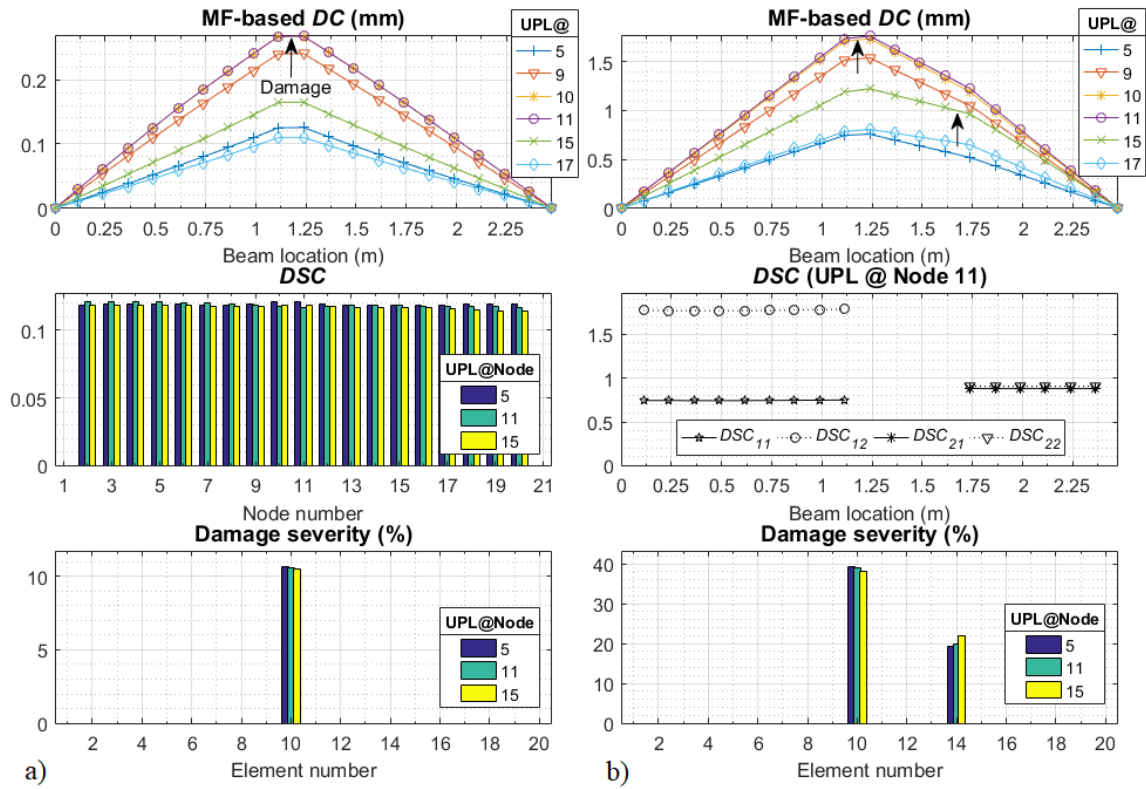
14 UPLs are summarised in Table 3.
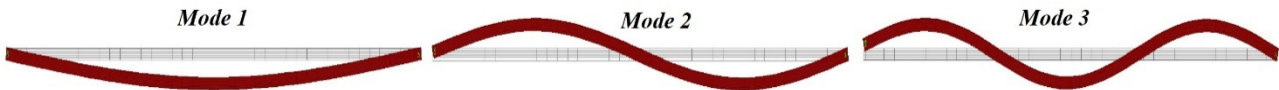
15

16 Fig. 4. The first three bending mode shapes in the undamaged state

17 Table 2. Natural frequencies of the beam FEM (Hz)

Mode No.	Intact	D1.1	D1.2	D1.3	D1.4	D1.5
1	16.58	16.48	16.37	16.06	15.95	15.73
2	65.13	65.12	65.12	65.10	64.40	63.27
3	142.86	142.14	141.15	138.84	138.57	138.22

18

Fig. 5. Numerical DD results using MF-based *DC*: (a) D1.1, (b) D1.4 (1st row: *DC* plots under UPLs at different nodes; 2nd and 3rd rows: *DSC* and damage severity under some selected UPLs)

For comparison, numerical damage quantification results from previous study using static deflection changes [25] are included in Table 3 and served as baseline for the present MF-based results. It shows that the dynamically estimated MF-based deflections can substitute the static deflections to locate and quantify the damage with minimal percentage errors of less than 5.5%.

Table 3. Damage quantification results from numerical MF-based *RDC* (damage extent: %)

Damage cases	D1.1	D1.2	D1.3	D1.4		D1.5	
				Damage 1	Damage 2	Damage 1	Damage 2
MF-based *RDC*	10.59	20.84	39.84	38.44	20.97	37.29	42.41
Static *RDC* [a]	10.41	20.71	39.96	39.31	20.56	39.40	41.70
Percentage error (%)	1.7%	0.6%	0.3%	2.2%	2.0%	5.4%	1.7%

[a] referenced numerical results from [25]

4. Experimental verification on the 2.5m steel beam

### 4.1. Test descriptions

Experimental verification of the proposed method is carried out on a 2.5m AS/NZS grade C450 cold formed

1   Duragal 75×40×4 CC beam as shown in Fig. 6. The dimensions and material properties of the beam are

2   essentially the same as those used for the analytical simulation (section 3). The beam was tested in order to

3   capture its vibration characteristics in the intact and the five damaged states as defined in Table 1. The data

4   acquisition system includes 21 lightweight 8630B5 Kistler piezoelectric accelerometers having 1V/g

5   sensitivity, ±5g input range and a broad frequency response range of 0.5-2000 Hz. It also includes a NI cDAQ-

6   9172 chassis, six NI-9234 bridge modules to form 21 single-axis accelerometer measurement channels. An in-

7   house LabVIEW professional app was used to read and log the data in a fully synchronized and automated

8   acquisition manner [32]. The transducers were attached to the upper surface of the beam to measure its vertical

9   acceleration under the sampling rate of 2048 Hz. Only 12 accelerometers as arranged in Fig. 7 are used in this

10   study for damage detection. Positions of the cuts and the actual dimensions of the beam cross section are also

11   illustrated in Fig. 7. Ambient vibration condition was created by randomly tapping the beam using a

12   lightweight rubber hammer. It should be noted that static deflection tests had been carried out on the same

13   model to validate the static DBDD method in the authors' previous study [25].
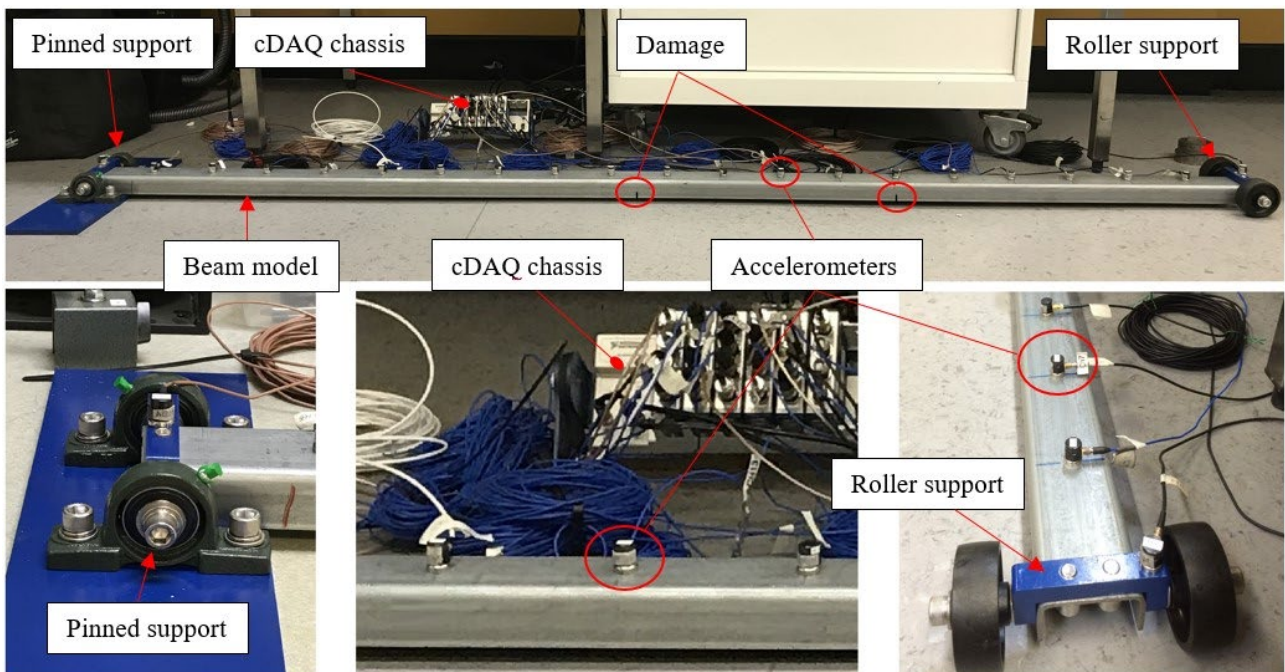
14

15   Fig. 6. The laboratory simply supported beam model

16   Modal parameters were estimated using the Enhanced Frequency Domain Decomposition (EFDD) method

17   from the OMA software ARTeMIS [33]. In all cases, the first four flexural modes can be clearly identified as

18   can be seen from Fig. 8. The un-scaled mode shapes in the undamaged state and the changes in natural

1 frequencies due to the progressive damage are presented in Fig. 9 and Table 4. It shows a good agreement with

2 those obtained numerically in Fig. 4 and Table 2.
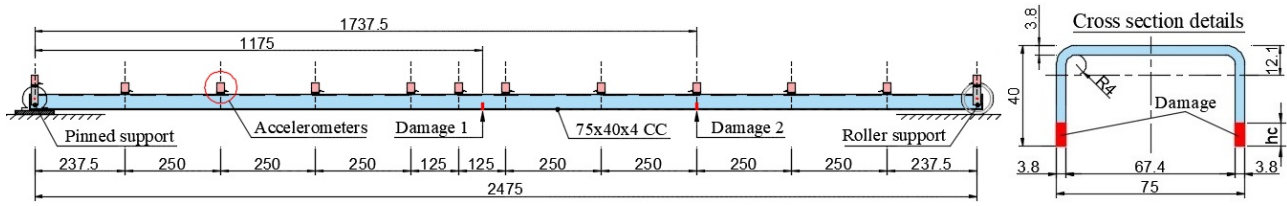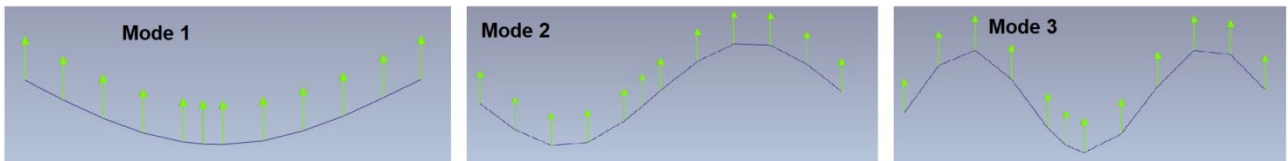
3

4 Fig. 7. Schematic diagram of the test model and the accelerometers used in this study (length in mm)

5 Table 4. Natural frequencies of the beam model (Hz)

Mode No.	Intact	D1.1	D1.2	D1.3	D1.4	D1.5
1	16.56	16.51	16.38	15.99	15.88	15.70
2	62.54	62.55	62.57	62.55	61.98	60.87
3	146.31	146.08	145.57	145.31	142.30	141.99
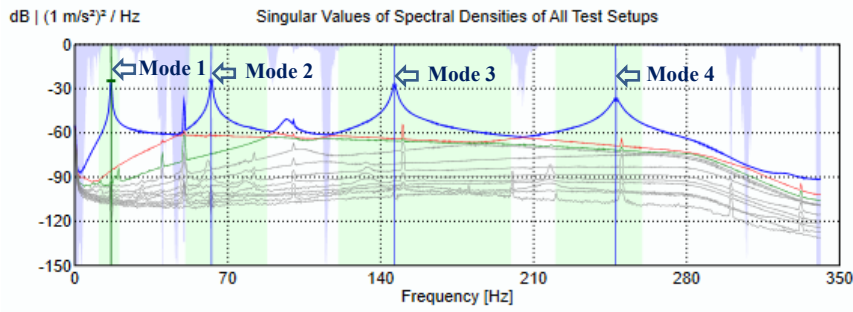
6

7

8 Fig. 8. A typical EFDD singular values for OMA of the 2.5m steel beam

9

10 Fig. 9. Plot of the first three mode shapes of the intact experimental beam

11 **4.2. Damage detection results using MF-based *DC* and *RDC***

12 The identified mode shapes were interpolated into 21 nodes at the same spacing as the numerical model (Fig.

13 3) using shape preserving piecewise cubic interpolation method. The mode shapes of the first three modes

14 were then mass-normalised using the mass matrix extracted from the validated FEM, before using to construct

15 the MF matrices and the subsequent MF-based deflections under 1kN virtual point loads. The MF-based DCs

16 and RDCs were then calculated and used to detect, locate and quantify the damages as presented in Fig. 10 to

13

1 Fig. 12.

2 Table 5 summarises the estimated damage extents, which are very close to the static deflection test results

3 carried out on the same model in previous study [25]. The table shows that the discrepancy between the two

4 methods is acceptable as the percentage errors are less than 11%.

5 Fig. 10 and Fig. 11 illustrate the damage detection results for the three single damage scenarios (D1.1 – D1.3).

6 Overall, the results agree well with those observed from numerical investigations (section 3). The main

7 difference should be noted is that the linearity of the MF-based DC plots for D1.1 and D1.2 was somewhat

8 affected by unavoidable measurement noise (Fig. 10, 1st row), and this subsequently resulted in noticeable

9 variations on the damage severity consistency plots (Fig. 10, 2nd row). However, when the damage was

10 significant enough in D1.3, it caused large DCs (about six times larger than those in D1.1) that outweighed the

11 noise, leading to a satisfactory linearity of the MF-based DC plot and consistent values on the DSC plot (Fig.

12 11). Even though the experimental DCs do not exactly follow the theoretical linear pattern in all cases, the

13 enhanced approach in this paper provides two other indicators that can help to reveal the damage. As can be

14 seen, all the DC plots depict clear peaks at the beam element No.10, and the intensity of the plots gradually

15 increases when the UPL is closer to nodes No.10 and 11. These two indications are sufficient to confirm the

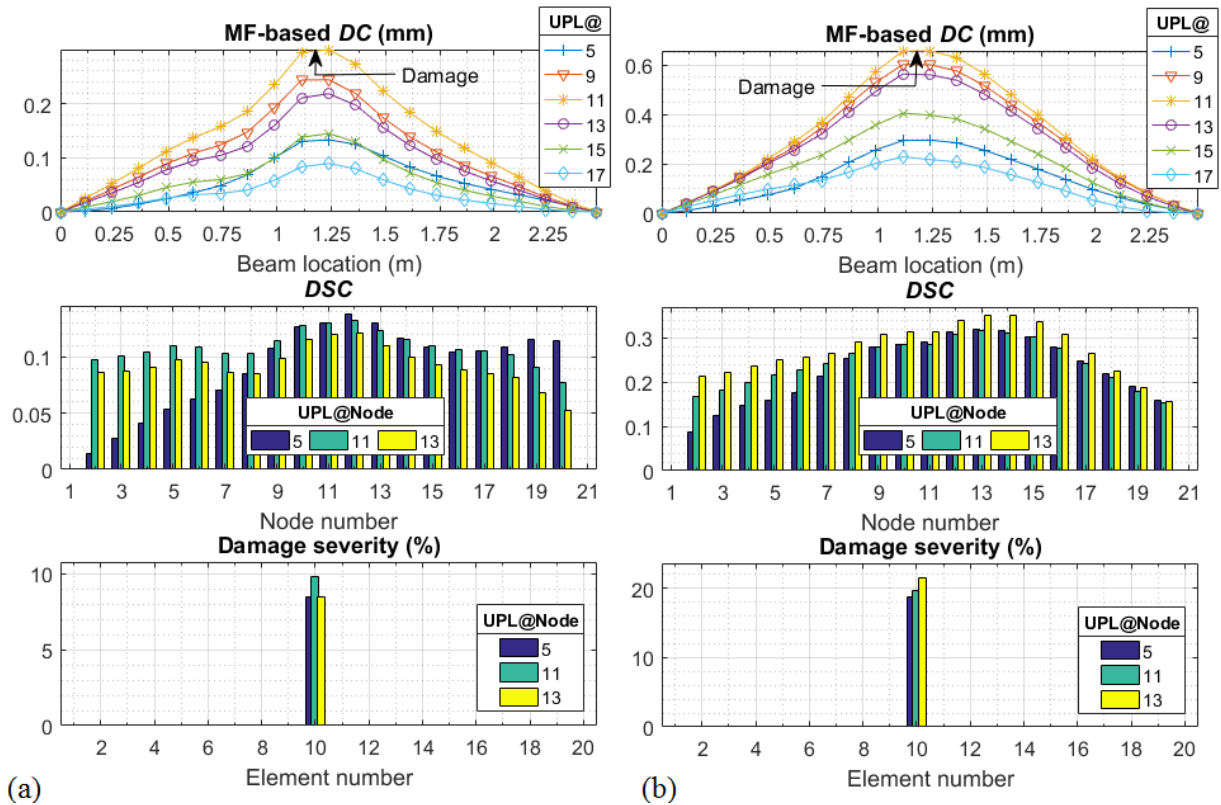16 presence of damage at the beam segment No.10.

Fig. 10. Experimental DD results: (a) D1.1, (b) D1.2

When the damage escalates to the two double damage scenarios, as can be observed from Fig. 12, measurement noise caused negligible nonlinearity of the *DC* plots, and insignificant variations on the consistency *DSC* plots. For the damage case D1.4 (Fig. 12a), the enhanced method successfully detects the second damage at beam element 14 by observing the *DC* plots under the UPLs at nodes 15 and 17. This is an important improvement since the original static DBDD method failed to detect this damage (Table 5). The enhanced method therefore can help to reduce the false negative detection rate. When the two damages are equally significant in the damage case D1.5, the enhanced DBDD method accurately locates and quantifies the damages regardless of the UPL used (Fig. 12b).
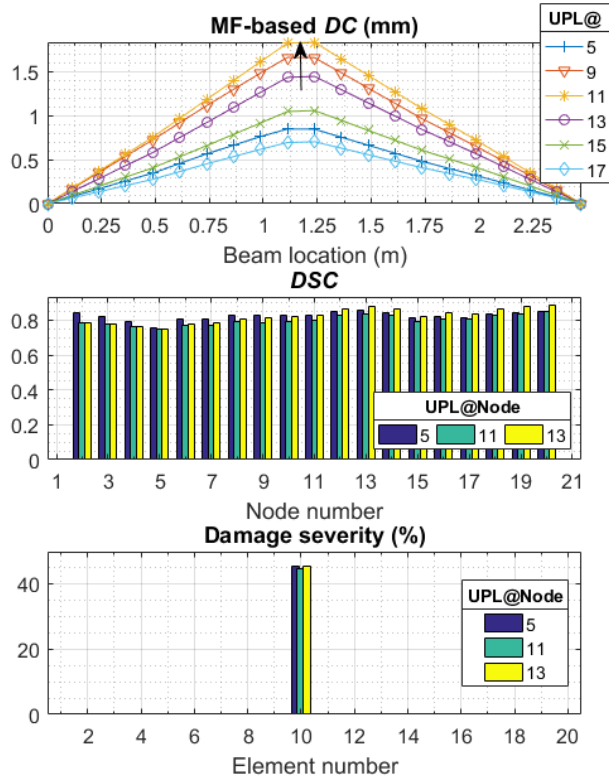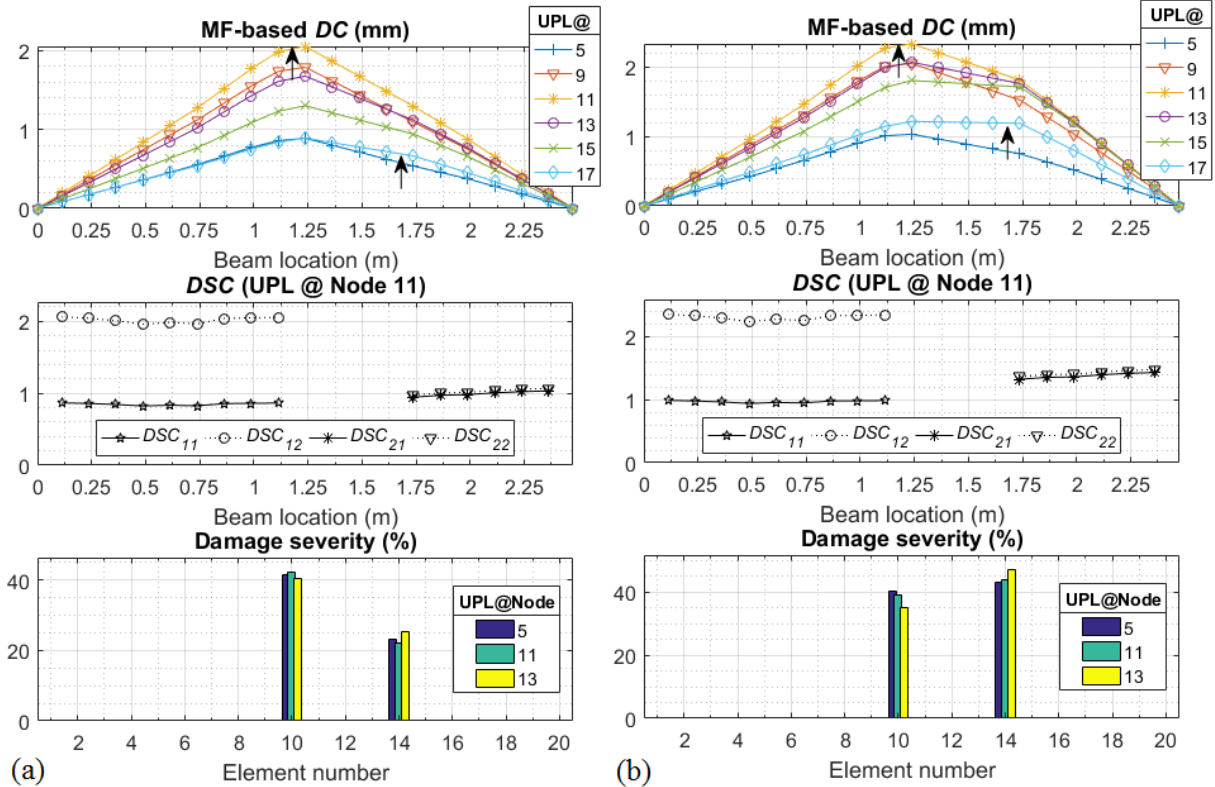
Fig. 11. Experimental DD results- D1.3

(a)   (b)

Fig. 12. Experimental DD results: (a) D1.4, (b) D1.5

Table 5. Damage quantification results from experimental MF-based *RDC* (damage extent: %)

16

Damage cases	D1.1	D1.2	D1.3	D1.4		D1.5	
				Damage 1	Damage 2	Damage 1	Damage 2
MF-based *RDC*	8.92	19.91	44.49	41.32	23.49	37.97	44.51
Static *RDC* [a]	9.19	22.33	41.51	43.90	Not detected	41.01	42.14
Percentage error (%)	2.9%	10.8%	7.2%	5.9%	N/A	7.4%	5.6%

1 *[a] referenced experimental results from [25]*

2 **4.3. Dealing with false positive detection**

3 From the damage detection results in the previous section, one might say that measurement noise may cause

4 abrupt changes at some undamaged elements on the MF-based *DC* plots in early damage scenarios, and that

5 this may lead to a false positive detection classifying those undamaged elements as being damaged. To assess

6 whether this can occur with the developed method, reconsider the damage case D1.1 where there is a noticeable

7 abrupt change at the beam element No.6 (Fig. 10a). This element is now suspected as being damaged (in

8 addition to the true damaged element 10) to provide a suspected double damage case (Fig. 13). Applying the

9 proposed damage quantification procedure, the damage severity coefficients of the two elements are calculated

10 and shown in the bottom graph of Fig. 13. It was found that the severity in the true damaged element 10 slightly

11 increased compared to the result in Fig. 10a, while in the suspected damaged element 6 the predicted value is

12 -4.0% in average. This negative value would allow the rejection of the hypothesis and once the suspected

13 damage is adjusted, the damage quantification process will be reinitiated in the form of a single damage case

14 and will therefore provide the same accurate results as presented in Fig. 10a. This shows that the proposed

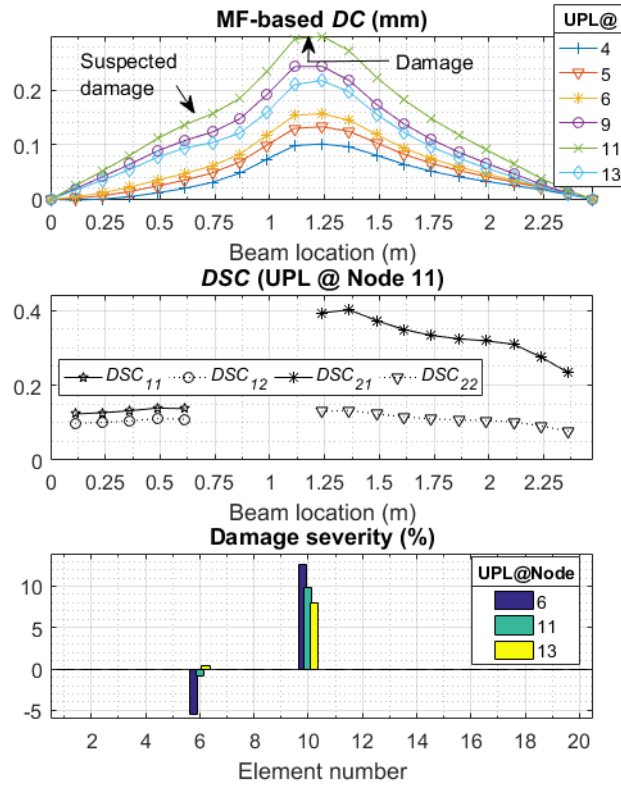15 method has an ability to eliminate false positive detection that may happen under the influence of noise.

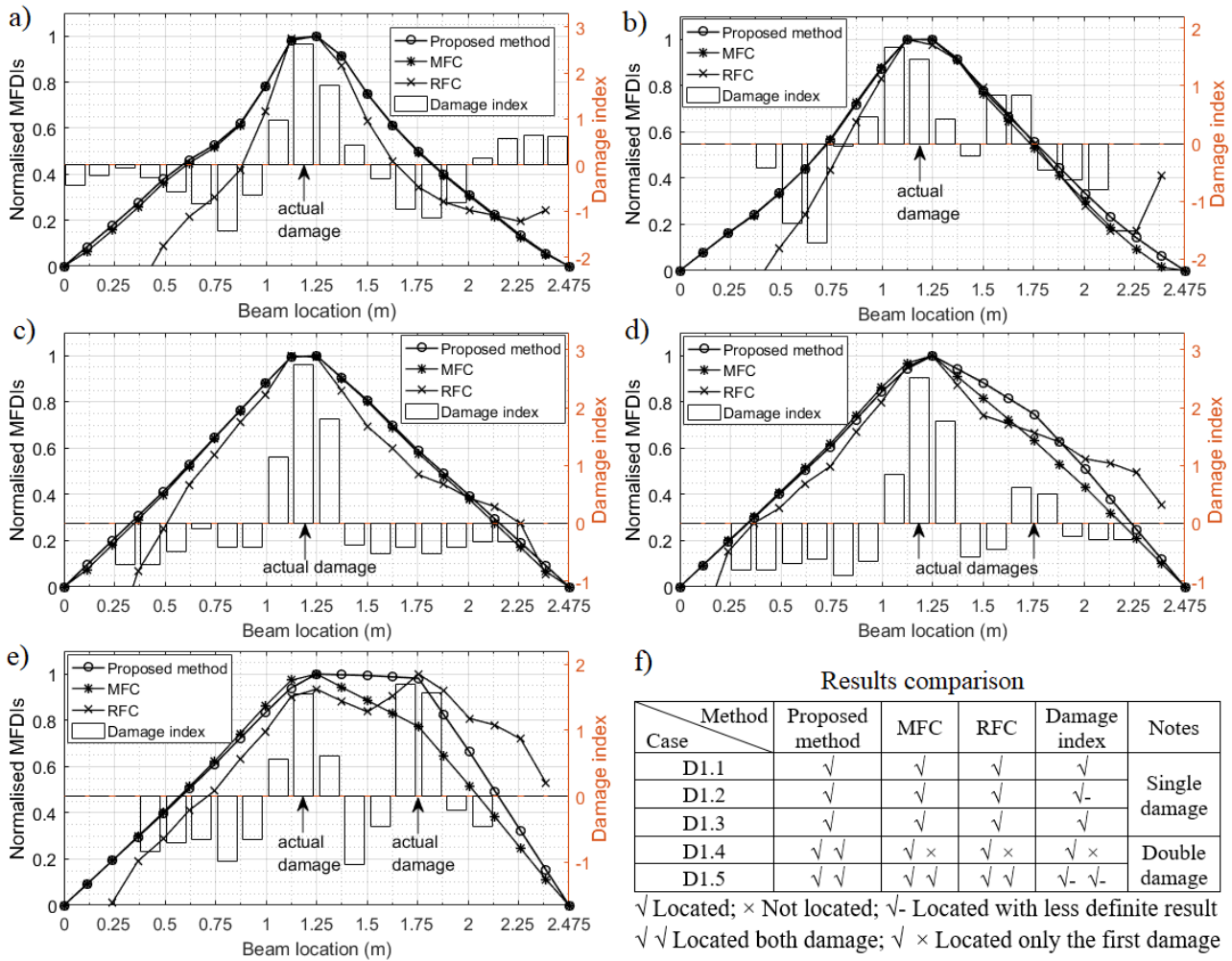Fig. 13. DD results including an undamaged element – D1.1

5. Comparative studies

In addition to the above comparison with the original DBDD method, the performance of the proposed method was also compared with three well-known vibration-based damage detection methods: (1) the modal flexibility change, or MFC, method [3], (2) the relative modal flexibility change (RFC) method [9], and (3) the modal strain energy (MSE) damage index method [34]. The first three modes from the above experimental study were used for all the four damage descriptors. For the MFC, RFC and the enhanced DBDD methods, the mode shapes were normalised with respect to the mass matrix extracted from the validated FEM (section 3). By contrast, the MSE damage index methods does not require this operation. To be comparable, the MFC index (column-wise maximum of the MFC matrix), the RFC index (diagonal entries of the RFC matrix) and the MF-based DC index (the proposed method) are normalised to be unity at their highest point. Damage is detected and located at the peaks of these normalised MF-based damage indices (MFDIs). For the MSE damage index method, the damage is located at elements whose damage index (Z) values greater than 2. In case Z is positive but lower than the threshold, the damage can be identified with low confidence level [34].

The damage identification results of the four methods are presented in Fig. 14a-e and summarised in Fig. 14f.

1   As can be observed from the figures, all the methods successfully identify the single damage cases D1.1 - D1.3

2   (Fig. 14a – c). The four methods can also identify the double damage case D1.5 when the severities of the two

3   damages are of the same level (Fig. 14e). However, when one of the damages is less severe than the other

4   (D1.4), only the proposed method can successfully identify both damages, while the other three methods can

5   only detect the larger one (Fig. 14d). In addition, it is noted that the damage detection results using MSE

6   damage index for D1.2 and D1.5 are somewhat less definite as the corresponding Z values are lower than the

7   confidence threshold, i.e. $Z < 2$ (Fig. 14b, e).

f) **Results comparison**

Case \ Method	Proposed method	MFC	RFC	Damage index	Notes
D1.1	√	√	√	√	Single damage
D1.2	√	√	√	√-	
D1.3	√	√	√	√	
D1.4	√ √	√ ×	√ ×	√ ×	Double damage
D1.5	√ √	√ √	√ √	√- √-	

√ Located; × Not located; √- Located with less definite result
√ √ Located both damage; √ × Located only the first damage

Fig. 14. Damage identification results from: the proposed IDBDD method, MFC, RFC, and damage index method
(a) D1.1, (b) D1.2, (c) D1.3, (d) D1.4, (e) D1.5, (f) Damage identification result comparison

11   A comparison between the proposed method and the MFC method is worth investigating as they both exploit

12   the changes in modal flexibility. The damage detection results of the two methods are almost identical for the

13   single damage cases (Fig. 14a – c). However, the difference lies in the double damage cases (Fig. 14d, e). By

14   scanning each column of the MFC matrix, the proposed method can select the most definite *DC* plots that

clearly reveal all possible damages. The traditional MFC method, on the other hand, only compares the maximum flexibility changes at all DOFs and hence the peak at the less severe damage can be easily masked by the peak at the more severe damage (Fig. 14d). The proposed method therefore provides a more robust tool to deal with multiple damages compared to the traditional MFC method.

It also should be emphasised that only the proposed method can accurately estimate the damage extents owing to the developed formulations of MF-based *DC* and *RDC* parameters with regard to the damage characteristics. The MSE damage index is also able to quantify the damage, but its accuracy is highly affected by measurement noise, and it normally requires rigorous optimization algorithms to improve the results [35].

From the comparisons, it is apparent that the proposed method performed better compared to the other three vibration-based methods in detecting and quantifying the damage, especially for the multiple damage cases.

6. Conclusions

This paper has presented an improved method to locate and quantify damage in beam-like structures and demonstrates its capability through comprehensive numerical and experimental investigations. The proposed method utilizes changes in indirect deflections estimated from modal flexibility (MF) matrices under multiple virtual unit point loads thereby providing several advantages compared to the existing methods. Since the deflections are estimated from modal parameters, the proposed approach can be used for monitoring in-service structures which provide obvious economic benefits for the asset owner. Next and most importantly, by using MF-based deflections instead of direct MF data, quantifying damage has now been available. From the result of numerical and experimental verifications, it was found that the damage detection results provided by the developed method agreed well with those obtained from the static deflection counterpart. In addition, the method developed in this paper has advantages compared to its predecessor since it provides an additional damage locating criterion that helped to identify early and multiple damages with higher confidence. Not only was the enhanced method robust against false negative detection, it was also capable of eliminating false positive detection. Finally, by comparing against three popular vibration-based damage detection methods i.e. MFC, RFC, and MSE damage index method, it was found that the proposed method had a superior performance in locating and quantifying the damage, especially for the multiple damage cases. Application of the method considering other practical circumstances is currently underway and will be reported in future work of the

authors.

References

1. Zingoni, A., *Structural health monitoring, damage detection and long-term performance.* Engineering structures, 2005. **12**(27): p. 1713-1714.
2. Chan, T.H.T. and D.P. Thambiratnam, *Structural health monitoring in Australia.* 2011: Nova Science Publishers.
3. Pandey, A.K. and M. Biswas, *Damage detection in structures using changes in flexibility.* Journal of Sound and Vibration, 1994. **169**(1): p. 3-17.
4. Pandey, A.K. and M. Biswas, *Experimental verification of flexibility difference method for locating damage in structures.* Journal of sound and vibration, 1995. **184**(2): p. 311-328.
5. Bernal, D., *Load vectors for damage localization.* Journal of Engineering Mechanics, 2002. **128**(1): p. 7-14.
6. Koo, K., S. Sung, J. Park, and H. Jung, *Damage detection of shear buildings using deflections obtained by modal flexibility.* Smart Materials and Structures, 2010. **19**(11): p. 115026.
7. Toksoy, T. and A. Aktan, *Bridge-condition assessment by modal flexibility.* Experimental Mechanics, 1994. **34**(3): p. 271-278.
8. Zhao, J. and J.T. DeWolf, *Sensitivity study for vibrational parameters used in damage detection.* Journal of structural engineering, 1999. **125**(4): p. 410-416.
9. Ni, Y., H. Zhou, K. Chan, and J. Ko, *Modal Flexibility Analysis of Cable‐Stayed Ting Kau Bridge for Damage Identification.* Computer‐Aided Civil and Infrastructure Engineering, 2008. **23**(3): p. 223-236.
10. Berman, A. and W.G. Flannelly, *Theory of incomplete models of dynamic structures.* AIAA journal, 1971. **9**(8): p. 1481-1487.
11. Nguyen, T., T.H.T. Chan, D.P. Thambiratnam, and L. King, *Development of a cost-effective and flexible vibration DAQ system for long-term continuous structural health monitoring.* Mechanical Systems and Signal Processing, 2015.
12. Aktan, A., K. Lee, C. Chuntavan, and T. Aksel. *Modal testing for structural identification and condition assessment of constructed facilities.* in *Proceedings-Spie the International Society for Optical Engineering.* 1994.
13. Doebling, S.W. and C.R. Farrar. *Computation of structural flexibility for bridge health monitoring using ambient modal data.* in *Proceedings of the 11th ASCE Engineering Mechanics Conference.* 1996. Citeseer.
14. Maeck, J. and G. De Roeck, *Damage assessment using vibration analysis on the Z24-bridge.* Mechanical Systems and Signal Processing, 2003. **17**(1): p. 133-142.
15. Shih, H.W., D.P. Thambiratnam, and T.H.T. Chan, *Damage detection in slab‐on‐girder bridges using vibration characteristics.* Structural Control and Health Monitoring, 2013. **20**(10): p. 1271-1290.
16. Duan, Z., G. Yan, J. Ou, and B. Spencer, *Damage localization in ambient vibration by constructing proportional flexibility matrix.* Journal of Sound and vibration, 2005. **284**(1): p. 455-466.
17. Koo, K., S.-H. Sung, and H.-J. Jung, *Damage quantification of shear buildings using deflections obtained by modal flexibility.* Smart Materials and Structures, 2011. **20**(4): p. 045010.
18. Sung, S., K. Koo, H. Jung, and H. Jung, *Damage-induced deflection approach for damage localization and quantification of shear buildings: validation on a full-scale shear building.* Smart Materials and Structures, 2012. **21**(11): p. 115013.
19. Le, N.T., D.P. Thambiratnam, T.H.T. Chan, A. Nguyen, and B.K.T. Huynh. *Damage assessment of concrete gravity dams using vibration characteristics.* in *6th International Conference on Structural Engineering, Mechanics and Computation, SEMC.* 2016.
20. Bernal, D., *Damage localization and quantification from the image of changes in flexibility.* Journal of Engineering Mechanics, 2013. **140**(2): p. 279-286.

21. Bakhtiari-Nejad, F., A. Rahai, and A. Esfandiari, *A structural damage detection method using static noisy data.* Engineering structures, 2005. **27**(12): p. 1784-1793.

22. Choi, I.-Y., J.S. Lee, E. Choi, and H.-N. Cho, *Development of elastic damage load theorem for damage detection in a statically determinate beam.* Computers & Structures, 2004. **82**(29): p. 2483-2492.

23. Wang, X., N. Hu, H. Fukunaga, and Z. Yao, *Structural damage identification using static test data and changes in frequencies.* Engineering structures, 2001. **23**(6): p. 610-621.

24. Yang, Q. and B. Sun, *Structural damage localization and quantification using static test data.* Structural health monitoring, 2011. **10**(4): p. 381-389.

25. Le, N.T., D.P. Thambiratnam, A. Nguyen, and T.H. Chan, *A new method for locating and quantifying damage in beams from static deflection changes.* Engineering Structures, 2019. **180**: p. 779-792.

26. Koo, K.Y., J.J. Lee, C.B. Yun, and J.T. Kim. *Damage detection in beam-like structures using deflections obtained by modal flexibility matrices.* in *Advances in Science and Technology.* 2008. Trans Tech Publ.

27. Bernagozzi, G., S. Mukhopadhyay, R. Betti, L. Landi, and P.P. Diotallevi, *Output-only damage detection in buildings using proportional modal flexibility-based deflections in unknown mass scenarios.* Engineering Structures, 2018. **167**: p. 549-566.

28. Ghali, A., A. Neville, and T.G. Brown, *Structural analysis: a unified classical and matrix approach.* 2014: CRC Press.

29. Doebling, S.W., C.R. Farrar, and M.B. Prime, *A summary review of vibration-based damage identification methods.* Shock and vibration digest, 1998. **30**(2): p. 91-105.

30. Wittrick, W., *A generalization of Macaulay's method with applications in structural mechanics.* AIAA Journal, 1965. **3**(2): p. 326-330.

31. Sinha, J.K., M. Friswell, and S. Edwards, *Simplified models for the location of cracks in beam structures using measured vibration data.* Journal of Sound and vibration, 2002. **251**(1): p. 13-38.

32. Nguyen, A., T.H.T. Chan, D.P. Thambiratnam, K.T.L. Kodikara, N.T. Le, and S. Jamali. *Output-only modal testing and monitoring of civil engineering structures: Instrumentation and test management.* in *SHMII 2017 - 8th International Conference on Structural Health Monitoring of Intelligent Infrastructure, Proceedings.* 2017.

33. SVS, *SVS-ARTeMIS Extractor-Release 5.3.* 2011, Aalborg-Denmark.

34. Kim, J.-T. and N. Stubbs, *Model-uncertainty impact and damage-detection accuracy in plate girder.* Journal of Structural Engineering, 1995. **121**(10): p. 1409-1417.

35. Nguyen, K.-D., T.H.T. Chan, and D.P. Thambiratnam, *Structural damage identification based on change in geometric modal strain energy–eigenvalue ratio.* Smart Materials and Structures, 2016. **25**(7): p. 075032.